

# SuperGSeg: Open-Vocabulary 3D Segmentation with Structured Super-Gaussians

Siyun Liang<sup>1†</sup> Sen Wang<sup>1†</sup> Kunyi Li<sup>1</sup> Michael Niemeyer<sup>2</sup> Stefano Gasperini<sup>1,3,4</sup>  
Nassir Navab<sup>1</sup> Federico Tombari<sup>1,2</sup>

<sup>1</sup>Technical University of Munich <sup>2</sup>Google <sup>3</sup>Munich Center for Machine Learning <sup>4</sup>Visual AI

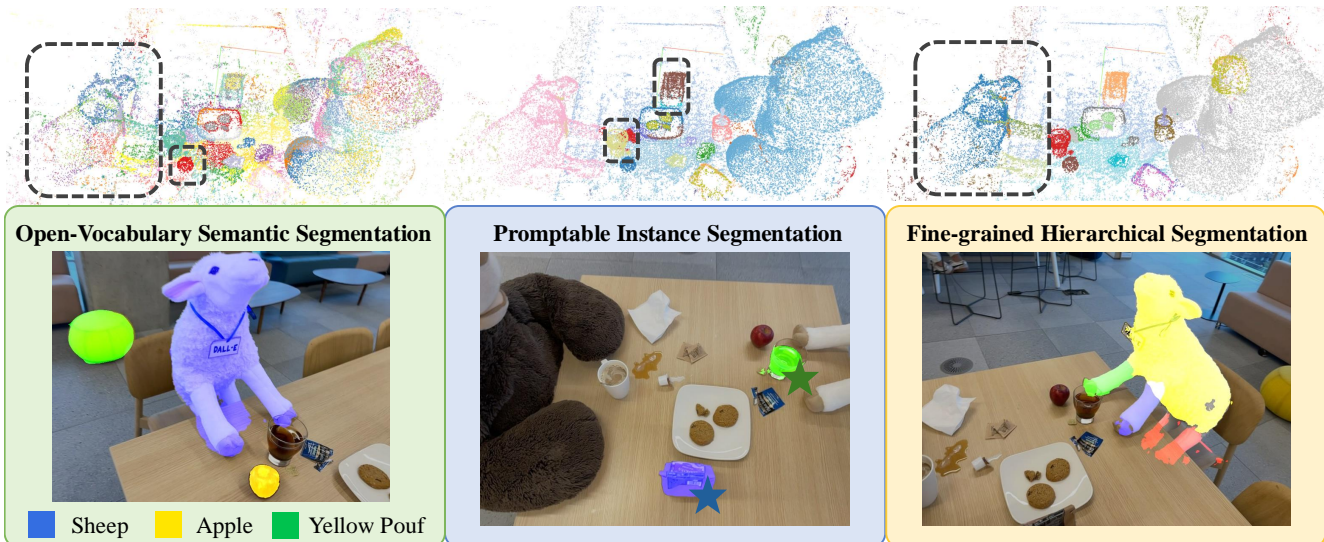


Figure 1. We present **SuperGSeg**, a novel method that clusters similar Gaussians into superpoint-like representations, termed Super-Gaussians. By leveraging Super-Gaussians, our approach effectively integrates diverse feature fields to achieve a comprehensive understanding of 3D scenes. SuperGSeg supports a wide range of functionalities, including open-vocabulary semantic segmentation, both promptable and promptless instance segmentation, and finer-grained hierarchical segmentation.

## Abstract

3D Gaussian Splatting has recently gained traction for its efficient training and real-time rendering. While the vanilla Gaussian Splatting representation is mainly designed for view synthesis, more recent works investigated how to extend it with scene understanding and language features. However, existing methods lack a detailed comprehension of scenes, limiting their ability to segment and interpret complex structures. To this end, we introduce *SuperGSeg*, a novel approach that fosters cohesive, context-aware scene representation by disentangling segmentation and language field distillation. *SuperGSeg* first employs neural Gaussians to learn instance and hierarchical segmentation features from multi-view images with the aid of off-the-shelf 2D masks. These features are then leveraged to create a sparse set of what we call *Super-Gaussians*. *Super-Gaussians* facilitate the distillation of 2D language features

into 3D space. Through *Super-Gaussians*, our method enables high-dimensional language feature rendering without extreme increases in GPU memory. Extensive experiments demonstrate that *SuperGSeg* outperforms prior works on both open-vocabulary object localization and semantic segmentation tasks. Please visit our [project](#) for more results.

## 1. Introduction

3D Gaussian Splatting (3DGS) [1] has rapidly gained recognition in novel view synthesis over NeRF [2] for its efficient training, real-time rendering, and explicit point-based representation. These attributes make 3DGS well-suited for a broad range of applications, such as 3D reconstruction [3–5], content generation [6], and scene understanding [7–11]. A particularly promising direction involves extending 3DGS frameworks to open-vocabulary understanding, empowering the interaction with the rendered scenes through flexible, language-based queries [12, 13].

<sup>†</sup>Equal contributions.

Significant efforts have been made to distill language features into 3DGS from both 2D [7, 9, 14, 15] and 3D [11] perspectives. 2D methods achieve this by transferring 2D language features to 3D through the multi-view consistency of 3DGS rendering, which is based on an explicit 3D point representation. To achieve this, they typically reduce the language feature maps from their original high dimensionality (e.g., 512D) to a lower dimension (e.g., 3D) [7] using an autoencoder or a convolutional network [9]. However, this dimensionality reduction can result in losing important information about language features. Another limitation of this approach is its inability to recognize occluded objects. OpenGaussian [11] addresses this issue by focusing on 3D point-level open-vocabulary tasks. By introducing a coarse-to-fine codebook optimized using masks generated by SAM [16], OpenGaussian assigns language features to instance-level Gaussian Splatting, enabling direct language queries on the 3D point cloud. However, two problems remain in OpenGaussian: 1) Only sparse language features can be queried at the 3D instance level, making pixel-level semantic segmentation tasks impractical. 2) Its decoupling of the alpha blending for language queries introduces challenges due to ambiguities in the language features assignment in regions with overlapping Gaussians, resulting in unreliable semantic predictions.

In this paper, we present a superpoint-guided language distillation method to improve fine-grained scene understanding in 3D environments. Building on LangSplat [7], we begin by generating pixel-space masks using an off-the-shelf segmentation model but move beyond fixed granularities, incorporating multi-level masks for enhanced detail capture in both instance and part segmentation. Our approach assigns each Gaussian instance and part features through contrastive learning [17], translating 2D segmentation insights into 3D. Inspired by Super points, we cluster Gaussians into *Super-Gaussians* based on spatial and instance characteristics, allowing for robust scene representation. By assigning high-dimensional language features to each Super-Gaussian, we support detailed, comprehensive scene understanding without loss of language information, enhancing structural integrity in complex scenes.

The main contributions of this paper are summarized as follows:

- We propose SuperGSeg: a 3D segmentation method with neural Gaussians, designed to learn hierarchical instance segmentation features from 2D foundation models.
- We introduce the concept of Super-Gaussian, a novel representation that integrates hierarchical instance segmentation features, enabling the embedding of high-dimensional language features. This approach addresses previously unfeasible challenges in representing complex scenes with rich semantic details.
- Extensive experiments on the LERF-OVS and ScanNet

datasets demonstrate the effectiveness of the proposed method, achieving significant improvements in open-vocabulary 3D object-level and scene-level semantic segmentation, with particular strength in capturing fine-grained scene details and dense pixel semantic segmentation tasks for the first time.

## 2. Related Work

**3D Gaussian Splatting** Neural Radiance Fields (NeRF) [2] combines neural implicit representations with differentiable volumetric rendering. In recent, 3D Gaussian Splatting (3DGS) [1] introduced a new explicit representation of 3D scenes via a set of 3D Gaussians. By optimizing their position and appearance, it leads to higher-quality renderings in real-time. Building on 3DGS, many recent works have focused on either enhancing the rendering quality [15, 18, 19] or the reconstruction performance [3–5]. While these approaches offer advantages in small-scale scenes, they tend to excessively expand Gaussian blobs to fit all training views, leading to redundancy and limiting scalability in complex, large-scale scenes. To overcome this, ScaffoldGS [20] introduced a hierarchical, region-aware 3D scene representation using anchor points, each linked to neural Gaussians with learnable offsets and attributes (opacity, color, rotation, scale) based on anchor features and view. The proposed SuperGSeg builds upon Scaffold-GS representation and brings it to a new level by embedding semantic and language features. Unlike prior works, this enables the query of the 3D scene via language and performs 3D semantic segmentation.

**Open-Set Segmentation** LERF [21] and related methods [22–24] embed language features [12] into 3D space to enable interactive open-vocabulary segmentation. However, since these language features are trained on full images without explicit boundary guidance, they often yield noisy segmentation boundaries and lack the ability to distinguish between instances due to missing instance-level supervision. SPInNeRF [25] addresses this by initializing 2D masks via video segmentation and lifting them into 3D with a NeRF [2], followed by multi-view refinement to achieve consistent 3D segmentation. Similarly, SA3D [26] introduces an online interactive segmentation method that propagates a SAM [16] mask into 3D and across other views iteratively. However, these approaches are sensitive to the choice of reference view and struggle with complex cases involving severe occlusions. OmniSeg3D [27] is a universal segmentation method that transforms inconsistent 2D segmentations into a globally consistent 3D feature field. It employs a hierarchical representation and contrastive learning framework, enabling robust hierarchical 3D understanding and high-quality object segmentation. However, OmniSeg3D builds upon NeRF, which requires longer training and does not integrate language features.

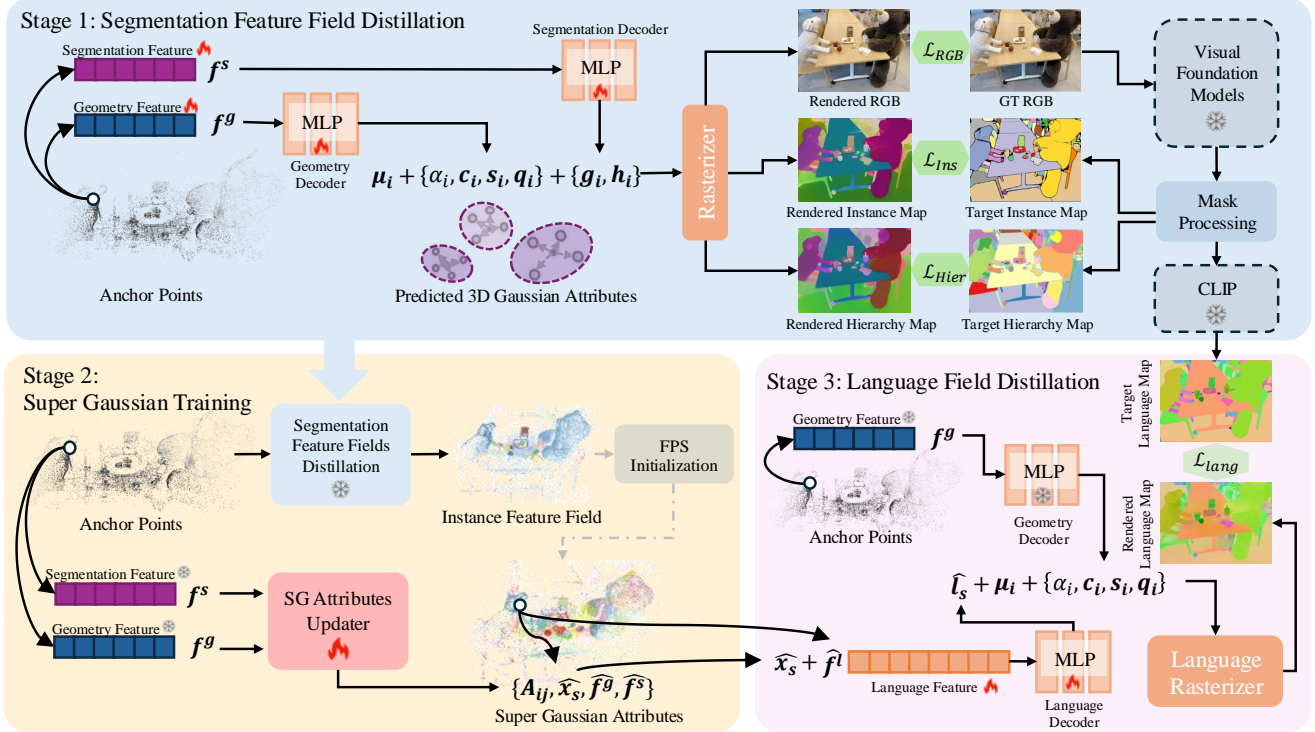


Figure 2. **SuperGSeg Overview.** We initialize the 3D Gaussians from a sparse set of anchor points, each generating  $k$  Gaussians with corresponding attributes. First, we train the appearance and segmentation features using RGB images and segmentation masks generated by SAM [16]. Next, we use the segmentation features and their spatial positions to produce a sparse set of Super-Gaussians, each carrying a 512-dimensional language feature. Finally, we train this high-dimensional language feature using a 2D feature map from CLIP [12].

**3D Open-Vocabulary Understanding** The significant advancements in universal 2D scene understanding, pioneered by SAM [16] and its variants, have motivated the exploration of integrating semantic features into 3D scene representations. Methods have been developed to incorporate language features of CLIP [12] or DINO [28] features into NeRF-based representations [21]. The success of 3DGS in novel view synthesis has inspired further research into extending its utility across diverse tasks. For example, LangSplat [7] employs a scene-wise language auto-encoder to learn scene-specific language features, providing clear object boundary distinctions in rendered feature images. Feature3DGS [9] introduces a parallel, N-dimensional Gaussian rasterizer to distill high-dimensional features for tasks such as scene editing and segmentation. To achieve cross-view consistency of 2D mask predictions, Gaussian Grouping [10] performs joint 3D reconstruction and segmentation of open-world objects, guided by SAM-based 2D mask predictions and 3D spatial constraints. However, they all failed to perform 3D language queries. OpenGaussian [11] enhances 3DGS for open-vocabulary understanding at the 3D point level. Associating high-dimensional, lossless CLIP features with 3D Gaussians enables consistent learning and distinctive features across and within objects. However, OpenGaussian de-

couples a language codebook from the Gaussian Splatting model, making it challenging to render per-pixel 2D language feature maps. In contrast, our method leverages both hierarchical and instance features from 2D inputs, integrating them into the rasterization pipeline to render per-pixel features. Additionally, we train a Super-Gaussian language field that incorporates both segmentation information and the geometric distribution of 3D Gaussians, achieving improved 3D segmentation and localization results.

### 3. Method

In this work, we present a novel framework for 3D scene reconstruction and understanding, named SuperGSeg. Starting with the structured Neural Gaussians (Section 3.1), we assign an instance feature and a hierarchical feature to each neural Gaussian to capture essential attributes related to semantic properties of the scene (Section 3.2). These features, combined with the spatial characteristics of each Gaussian point, are then used to learn the Super-Gaussians through an online point clustering method (Section 3.3). We design this over-segmented Super-Gaussian representation to facilitate learning fine-detailed language features (Section 3.4), effectively bridging the gap between spatial precision and semantic richness.

### 3.1. Neural Gaussian Splatting

3D Gaussian Splatting (3DGS) [1] employs a set of 3D points to effectively render images from given viewpoints, each characterized by a Gaussian function with 3D mean  $\boldsymbol{\mu}_i \in \mathbb{R}^3$  and covariance matrix  $\boldsymbol{\Sigma}_i \in \mathbb{R}^{3 \times 3}$ :

$$o_i(\mathbf{x}) = \alpha_i * \exp\left(-\frac{1}{2}(\mathbf{x} - \boldsymbol{\mu}_i)^T \boldsymbol{\Sigma}_i^{-1}(\mathbf{x} - \boldsymbol{\mu}_i)\right). \quad (1)$$

Given a 3D position  $\mathbf{x}$ ,  $o_i(\mathbf{x})$  represents current contribution by the  $i$ -th Gaussian weighted by its opacity  $\alpha_i$ . To facilitate optimization,  $\boldsymbol{\Sigma}_i$  is factorized into the product of a scaling matrix  $\mathbf{S}_i$ , represented by scale factors  $\mathbf{s}_i \in \mathbb{R}^3$ , and a rotation matrix  $\mathbf{R}_i$  encoded by a quaternion  $\mathbf{q}_i \in \mathbb{R}^4$ :

$$\boldsymbol{\Sigma}_i = \mathbf{R}_i \mathbf{S}_i \mathbf{S}_i^T \mathbf{R}_i^T. \quad (2)$$

3D Gaussians are then projected onto a 2D image plane according to elliptical weighted average (EWA) [29] to render images for given views. Color map  $\hat{\mathbf{C}}(\mathbf{u})$ , feature maps  $\hat{\mathbf{G}}(\mathbf{u})$  or  $\hat{\mathbf{H}}(\mathbf{u})$  at pixel  $\mathbf{u}$  is rendered by  $N$  projected and ordered Gaussians using point-based  $\alpha$ -blending:

$$\{\hat{\mathbf{C}}, \hat{\mathbf{G}}, \hat{\mathbf{H}}\}(\mathbf{u}) = \sum_{i \in N} T_i o_i \{\mathbf{c}_i, \mathbf{g}_i, \mathbf{h}_i\}, \quad (3)$$

where  $T_i = \prod_{j=1}^{i-1} (1 - o_j)$ ,  $\mathbf{c}_i$  is the color vector, and  $\mathbf{g}_i, \mathbf{h}_i$  are instance feature and hierarchical feature vector assigned to  $i$ -th Gaussian.

Assigning each Gaussian with high-dimension features is inefficient. Instead, we apply neural Gaussian as Scaffold-GS [20] by voxelizing the input point cloud to a sparse set of anchor points, where each anchor is parametrized with a 3D position  $\mathbf{x}$ , a geometry feature  $\mathbf{f}^g \in \mathbb{R}^{32}$  and a segmentation feature  $\mathbf{f}^s \in \mathbb{R}^{32}$  (Section 3.2). The geometry feature  $\mathbf{f}^g$  of each anchor is then passed through several multi-layers perceptrons (MLPs)  $\{F_\alpha, F_c, F_q, F_s\}$  to spawn the attributes of  $k$  predicted Gaussians  $\{(\alpha, \mathbf{c}, \mathbf{q}, \mathbf{s})_i | i = 0, \dots, k-1\}$ , respectively. While the segmentation feature  $\mathbf{f}^s$  predicts additional instance and hierarchical feature  $\{(\mathbf{g}, \mathbf{h})_i | i = 0, \dots, k-1\}$  for each Gaussian via MLP  $\{F_g, F_h\}$ . The 3D means of neural Gaussians are calculated as:

$$\{\boldsymbol{\mu}_0, \dots, \boldsymbol{\mu}_{k-1}\} = \mathbf{x} + \{\mathbf{O}_0, \dots, \mathbf{O}_{k-1}\} \cdot l, \quad (4)$$

where  $\mathbf{x}$  is the position of the anchor and  $l$  the scaling factor associated with that anchor, while  $\{\mathbf{O}_0, \dots, \mathbf{O}_k \in \mathbb{R}^{k \times 3}\}$  are the learnable offsets.

### 3.2. Segmentation Feature Field Distillation

**SAM Mask Processing.** Given an image, SAM [16] can generate a set of 2D binary segmentation masks, denoted as  $\mathcal{M}_{sam} = \{\mathbf{M}_m \in \mathbb{R}^{H \times W} \mid m = 1, \dots, |\mathcal{M}_{sam}|\}$ . However, these masks lack inherent multi-view consistency, leading to ambiguous instance information across different views. In particular, overlapping masks within  $\mathcal{M}_{sam}$  can result in pixels that belong to multiple masks simultaneously. This ambiguity undermines the hierarchical structure, making it challenging to distinguish distinct parts and model their relationships effectively.

To address this issue, we adopt a hierarchical representation [27]. Starting with dividing any overlapping regions in  $\mathcal{M}_{sam}$  into distinct patches, denoted as  $\mathcal{P}_{hier}$ . Each patch represents a group of pixels that share the same set of overlapping masks. This approach assigns each pixel to a unique patch, ensuring non-overlapping segmentation. We then construct a correlation matrix between these patches. For each pair of patches  $\mathbf{P}_i$  and  $\mathbf{P}_j$ , we define their correlation as the number of masks that cover both patches:

$$\sum_{m=1}^{|\mathcal{M}_{sam}|} \mathbb{1}(\mathbf{P}_i \subseteq \mathbf{M}_m) \cdot \mathbb{1}(\mathbf{P}_j \subseteq \mathbf{M}_m). \quad (5)$$

The more shared masks, the stronger the correlation between the two patches. In contrast, if two patches do not share any masks, their correlation is zero. We further group the patches into non-overlap instance masks  $\mathcal{M}_{ins}$ .

**Instance and Hierarchical Feature Field** Previous methods [7, 8] focus on a single level of granularity, and extending this to learn multiple feature fields simultaneously at different levels is challenging due to the high memory demands. Ours addresses this by efficiently learning both instance- and hierarchical-level feature fields, enabling comprehensive scene understanding and reconstruction.

To distill both instance and hierarchical feature fields, we first decode the segmentation feature  $\mathbf{f}^s$  of each anchor into  $k$  instance features  $\mathbf{g}$  and  $k$  hierarchical features  $\mathbf{h}$ . Given a camera view, the current instance feature map  $\hat{\mathbf{G}} \in \mathbb{R}^{16 \times H \times W}$  and the hierarchical feature map  $\hat{\mathbf{H}} \in \mathbb{R}^{16 \times H \times W}$  can be rendered following the spawning of attributes and the 3D Gaussian rasterization process defined in Section 3.1.

To supervise the instance and hierarchical feature field and maintain the multi-view consistency, we employ contrastive learning following OmniSeg3D [27]. For instance-level contrastive learning, features within the same instance mask should be similar, whereas features belonging to different instance masks should be distinct. For instance mask  $p$ , its set of rendered instance features is  $\{\mathbf{g}^p\}$ , and the mean feature is  $\bar{\mathbf{g}}^p$ . The contrastive loss  $\mathcal{L}^{p,t}(r)$  between the instance mask  $p$  and  $r$ , calculating with  $t$ -th features in set  $\{\mathbf{g}^p\}$  is defined as:

$$\mathcal{L}^{p,t}(r) = -\log \frac{\exp(\mathbf{g}_t^p \cdot \bar{\mathbf{g}}^r / \tau_r)}{\sum_{q=1}^{|\mathcal{M}_{ins}|} \exp(\mathbf{g}_t^p \cdot \bar{\mathbf{g}}^q / \tau_q)}, \quad (6)$$

where  $\tau$  is the temperature of the contrastive loss. Which gives the instance feature loss:

$$\mathcal{L}_g = \frac{1}{|\mathcal{M}_{ins}|} \sum_{p=1}^{|\mathcal{M}_{ins}|} \sum_{t=1}^{|\{\mathbf{g}^p\}|} \mathcal{L}^{p,t}(p). \quad (7)$$

and the hierarchical feature loss [27] can be written as:

$$\mathcal{L}_h = \sum_{p=1}^{|\mathcal{P}_{hier}|} \sum_{d=1}^{d_{\max}^p} \mathcal{L}_{p,d}, \quad (8)$$

$$\mathcal{L}_{p,d} = \frac{\lambda^{d-1}}{|\mathcal{R}_d^p|} \sum_{t=1}^{|\{h^p\}|} \sum_{r \in \mathcal{R}_d^p} \max(\mathcal{L}^{p,t}(r), \mathcal{L}_{\max}^{p,t}(d-1)), \quad (9)$$

where  $\lambda^{d-1}$  is a hyperparameter,  $\mathcal{R}_d^p$  represents the patch index set at level  $d$  of patch  $p$ , and  $r \in \mathcal{R}_d^p$  refers to a patch at level  $d$ . The maximum loss at level  $d$  ensures that the contrastive loss between the pixel feature  $t$  and patches with higher correlation (lower  $d$ ) is always smaller than for patches with lower correlation [27]:

$$\mathcal{L}_{\max}^{p,t}(d) = \max_{r \in \mathcal{R}_d^p} \mathcal{L}^{p,t}(r). \quad (10)$$

The overall loss for the first stage is:

$$\mathcal{L}_{stage1} = \mathcal{L}_c + \lambda_g \mathcal{L}_g + \lambda_h \mathcal{L}_h. \quad (11)$$

with  $\mathcal{L}_c$  as L1 loss between rendered and GT RGB images.

### 3.3. Feature Distillation with Super-Gaussian

Optimizing language features for each Gaussian [7–9] can lead to semantic inconsistencies within objects, especially when occluded. Averaging language features across viewpoints introduces conflicting supervision signals, resulting in noisy feature distillation. To address this, we propose the Super-Gaussian (SuperG), a sparse scene representation with high-dimensional language features enabling efficient feature distillation.

**Super-Gaussian Initialization.** To initialize the Super-Gaussians, we apply the Farthest Point Sampling (FPS) algorithm. We initialize  $S$  Super-Gaussians, each with an initial coordinate  $\hat{\mathbf{x}}_s$ , a segmentation feature  $\hat{\mathbf{f}}^s$  and a geometry feature  $\hat{\mathbf{f}}^g$ . For  $i$ -th anchor, we compute its nearest  $k$  Super-Gaussian as set  $\mathcal{N}_i$ . The association probability [30, 31] between the  $i$ -th anchor and the  $j$ -th Super-Gaussian ( $j \in \mathcal{N}_i$ ) is computed as:

$$\mathbf{A}_{ij} = F_{sg} \left( \phi(\mathbf{x}_i, \hat{\mathbf{x}}_j) \parallel \varphi(\mathbf{f}_i^s, \hat{\mathbf{f}}_j^s) \parallel \psi(\mathbf{f}_i^g, \hat{\mathbf{f}}_j^g) \right), \quad (12)$$

where  $\phi$ ,  $\varphi$ , and  $\psi$  are functions for weighting the relevancy. For instance,  $\phi(\mathbf{x}_i, \hat{\mathbf{x}}_j)$  is defined as:

$$\phi(\mathbf{x}_i, \hat{\mathbf{x}}_j) = F_\phi(\mathbf{x}_i - \hat{\mathbf{x}}_j), \quad (13)$$

The weighting function  $\phi$  computes the weight of the SuperG based on the difference in position between an anchor and the SuperG. Similarly,  $\varphi$  and  $\psi$  compute weights based on segmentation and geometry features distance, respectively. These weights are concatenated and used as input to the final SuperG prediction MLP,  $F_{sg}$ . The anchor-SuperG association  $\mathbf{A}_{ij}$  is then normalized using softmax.

**Super-Gaussian Update.** We iteratively update the  $j$ -th SuperG based on the latest normalized association map  $\mathbf{A} \in \mathbb{R}^{N \times k}$ ,  $N$  is the number of anchors. Its position is computed as the normalized weighted sum of the anchor points influencing it:

$$\hat{\mathbf{x}}_j = \frac{1}{\sum_{j=i}^n \mathbb{I}(j \in \mathcal{N}_i) \mathbf{A}_{ij}} \sum_{i=1}^N \mathbb{I}(j \in \mathcal{N}_i) \mathbf{A}_{ij} \mathbf{x}_i. \quad (14)$$

The average anchor segmentation features and geometry features of each SuperG are updated similarly.

We apply a reconstruction loss to reconstruct the anchor attributes based on the current SuperG attributes and their assignments, minimizing the difference between the reconstructed attributes and the original ones:

$$\mathcal{L}_{recon, \mathbf{x}} = \frac{1}{N} \sum_{i=1}^N \|\mathbf{x}_i\|, \sum_{j \in \mathcal{N}_i} \mathbf{A}_{ij} \hat{\mathbf{x}}_j\|. \quad (15)$$

However, the reconstruction loss alone cannot guarantee that the Super-Gaussians remain compact. Anchors belonging to the same Super-Gaussian could be close in the instance feature space while being spatially distant, particularly when two instances never appear together in the same view to be optimized by the contrastive loss. To address this issue, we apply this compactness loss:

$$\mathcal{L}_{compact, \mathcal{X}} = \frac{1}{S} \sum_{j=1}^S \|\mathcal{X}_j - \hat{\mathbf{x}}_j\|, \quad (16)$$

where  $\hat{\mathbf{x}}_j$  refers to the position of each SuperG, and  $\mathcal{X}_j$  represents the set of coordinates of anchors that have the  $j$ -th SuperG as their neighbor. Note that during this stage, we optimize only the Super-Gaussian association modules while keeping the anchor positions and features fixed.

### 3.4. Language Field Distillation

A learnable latent language feature vector  $\hat{\mathbf{f}}^l \in \mathbb{R}^{32}$  is assigned to each SuperG, then is passed through a language decoder  $F_L$  together with its coordinate  $\hat{\mathbf{x}}_s \in \mathbb{R}^3$  to map to a CLIP analogous language feature  $\hat{\mathbf{l}}_s = F_L(\hat{\mathbf{f}}^l, \hat{\mathbf{x}}_s)$ . We convert the soft association map  $\hat{\mathbf{A}} \in \mathbb{R}^{n \times k}$  into a hard assignment map  $\hat{\mathbf{A}} \in \mathbb{Z}^n$ . The rasterizer is modified to render the 512D language feature map  $\hat{\mathbf{L}}$  using the SuperG language features and the assignment map. We freeze all other MLPs and properties, optimizing only the latent language feature vector per SuperG, along with the language decoder, using a cosine similarity loss with the 2D CLIP feature extracted for each instance mask  $\mathbf{L}$ .

$$\mathcal{L}_{lang} = 1 - \cos(\hat{\mathbf{L}}, \mathbf{L}). \quad (17)$$

## 4. Experiments

### 4.1. Experimental Setup

**Datasets.** We evaluate our method on the **open-vocabulary novel view semantic segmentation and object selection tasks** on the ScanNet v2 [32] and LERF-OVS [7] datasets. ScanNet v2 [32] includes posed RGBD images and 2D semantic labels of indoor scenes. We randomly select 8 scenes from the entire scene sequence. These include a

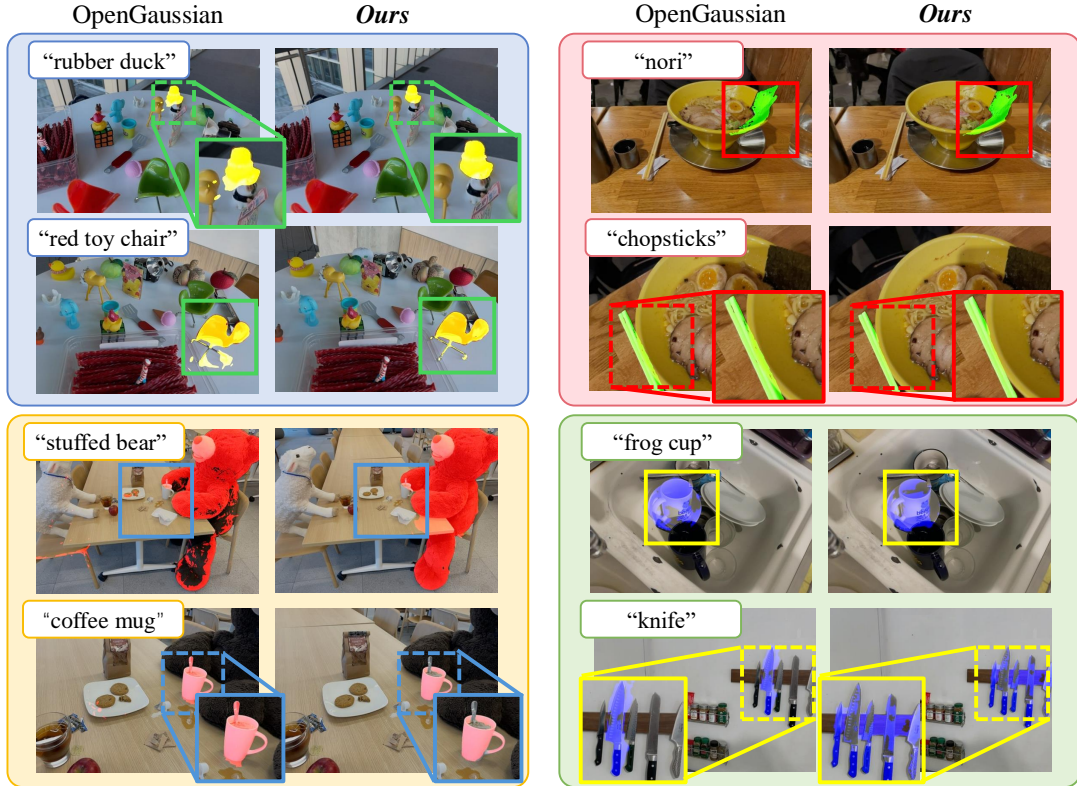


Figure 3. Qualitative comparison on the 4 scenes of the LERF-OVS dataset [21] for the open-vocabulary 3D object selection task. The proposed SuperGSeg is compared with OpenGaussian [11]. Text queries for each scene are displayed in quotation marks. SuperGSeg delivers more precise and less noisy segmentation masks.

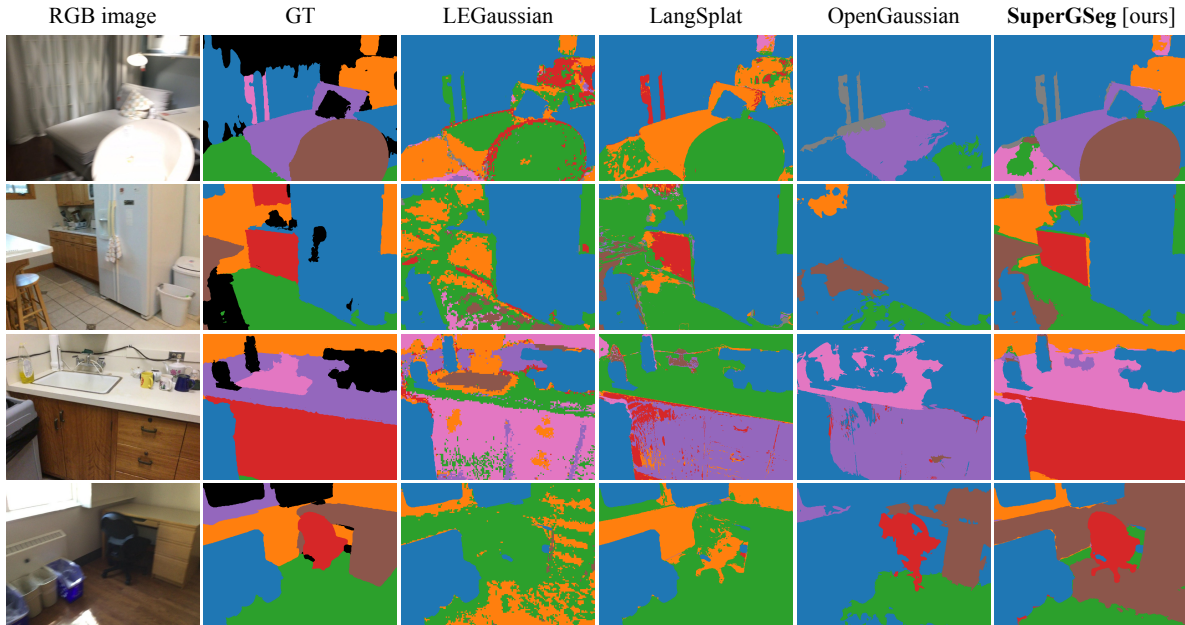


Figure 4. Qualitative comparison of semantic segmentation predictions on the ScanNet v2 dataset [32].

variety of indoor environments, e.g., living rooms, bedrooms, kitchens, and offices. For each scene, we split the data into a training set (composed of every 20th image from the original sequence) and a test set (derived from

the intermediate images between the training set samples). For semantic segmentation, we specifically use the 20 object categories. LERF-OVS is an extension of the LERF dataset [7], which consists of complex in-the-wild scenes

Method	mIoU mAcc		mIoU mAcc		mIoU mAcc		mIoU mAcc		mIoU mAcc		mIoU mAcc		mIoU mAcc	
	mean		wall		floor		cabinet		table		desk		curtain	
LEGaussians [8]	8.7	33.2	17.9	53.1	14.6	20.6	2.7	18.6	0.0	0.0	0.5	13.5	1.9	10.4
OpenGaussian [11]	24.1	68.7	13.4	<b>96.6</b>	31.2	74.4	0.3	22.9	0.1	1.0	<b>30.6</b>	<b>35.6</b>	17.7	<b>79.2</b>
LangSplat [7]	27.6	48.3	45.3	72.6	43.3	45.6	24.8	56.7	21.9	<b>87.4</b>	0.1	6.4	46.8	66.5
<b>SuperGSeg [ours]</b>	<b>54.7</b>	<b>74.7</b>	<b>58.8</b>	92.9	<b>53.6</b>	<b>86.5</b>	<b>69.8</b>	<b>83.8</b>	<b>35.7</b>	54.8	15.0	<b>16.7</b>	<b>61.8</b>	64.5
	<i>toilet</i>		<i>counter</i>		<i>refrigerator</i>		<i>chair</i>		<i>sink</i>		<i>window</i>		<i>door</i>	
LEGaussians [8]	13.7	16.3	10.7	27.0	9.0	74.3	0.4	28.7	0.3	0.4	0.0	44.4	1.4	4.7
OpenGaussian [11]	<b>73.0</b>	<b>98.4</b>	3.0	9.3	<b>88.0</b>	<b>98.3</b>	36.5	83.4	3.0	3.7	<b>75.0</b>	<b>88.8</b>	<b>75.4</b>	<b>97.0</b>
LangSplat [7]	0.1	5.4	10.7	34.7	0.7	33.3	18.0	48.5	0.0	0.0	0.0	0.1	55.6	66.3
<b>SuperGSeg [ours]</b>	26.9	26.9	<b>14.0</b>	<b>59.1</b>	79.4	80.2	<b>80.4</b>	<b>83.8</b>	<b>11.7</b>	<b>12.0</b>	54.7	77.0	58.2	58.3

Table 1. Comparison of mIoU and mAcc for various methods on each class of the ScanNet v2 dataset [32].

Method	mean		<i>figurines</i>		<i>teatime</i>		<i>ramen</i>		<i>waldo_kitchen</i>	
	mIoU	mAcc	mIoU	mAcc	mIoU	mAcc	mIoU	mAcc	mIoU	mAcc
LangSplat [7]	9.66	12.41	10.16	8.93	11.38	20.34	7.92	11.27	9.18	9.09
LEGaussians [8]	16.21	23.82	17.99	23.21	19.27	27.12	15.79	26.76	11.78	18.18
OpenGaussian [11]	<b>38.36</b>	51.43	39.29	55.36	<b>60.44</b>	76.27	<b>31.01</b>	<b>42.25</b>	22.70	31.82
<b>SuperGSeg [ours]</b>	35.94	<b>52.02</b>	<b>43.68</b>	<b>60.71</b>	55.31	<b>77.97</b>	18.07	23.94	<b>26.71</b>	<b>45.45</b>

Table 2. 3DGS-based open-vocabulary semantic segmentation comparison on the LERF-OVS dataset [7].

captured with consumer-level devices. LERF-OVS is annotated with ground truth masks for textual queries to enable open-vocabulary 3D semantic segmentation and object localization.

**Baselines and Metrics.** For baselines, we compare our method with three recent Gaussian Splatting-based approaches: LangSplat [7], Legaussian [8], and OpenGaussian [11]. For the open-vocabulary object selection task, we use a similar strategy as [11]. We first group SuperGaussians into class-agonistic instances and then perform text queries in 3D space. The queried Super-Gaussians vote for corresponding instances, which are rendered into 2D query masks. For the open vocabulary semantic segmentation task, we query the text prompts based on the class names and compute the cosine similarities with the learned feature maps, as described in [9], to generate the predicted semantic maps. We then evaluate the results by calculating the mean Intersection over Union (mIoU) and mean accuracy (mAcc) for 20 classes from the ScanNet dataset.

**Implementation Details.** We use the SAM ViT-H model to generate 2D masks from input images and then extract language features for each instance mask using the OpenCLIP ViT-B/16 model following [7]. The training process is divided into three stages. In the first stage, we train the Scaffold-GS [20] with instance and hierarchical feature attributes for 30k iterations. In the second stage, we freeze the geometry and multi-granularity features network from stage one and train only the SuperG clustering network for another 30k iterations. Finally, in the last stage, we freeze all other parameters and optimize the language features for each SuperG for 10k iterations. We use Adam [33] opti-

mizer for the MLPs with an initial learning rate of 0.01 and an exponential annealing schedule of 0.001 as in [34].

## 4.2. Results on the ScanNet Dataset

**Quantitative Results.** As shown in Table 1, it is evident that SuperGSeg outperforms all other methods, achieving an impressive mean mIoU and mAcc. These results demonstrate the effectiveness of our method in capturing the open vocabulary semantic information of the scene, yielding superior performance in a variety of object categories. In contrast, LEGaussian [15] achieves significantly lower scores, with mIoU and mAcc, respectively. This highlights the limited ability of LEGaussian to generalize across multiple object categories, with particularly poor performance on more complex objects such as desks and toilets. Similarly, LangSplat [7] also demonstrates fair performance, indicating that while it performs better than LEGaussian, it still struggles with diverse object categories. OpenGaussian [11] shows a mixed performance, with relatively high mIoU and mAcc in certain categories, notably wall, floor, and toilet, but it lags behind SuperGSeg in overall scene understanding. For example, OpenGaussian achieves a high mIoU and mAcc for the toilet class, but it suffers from poor performance on objects like the desk and sink, where it scores near zero.

**Qualitative Results.** As shown in Figure 4, our proposed method delivers significantly better masks than prior works. While OpenGaussian [11] demonstrates competitive performance in 3D object-level semantic segmentation, it fails in dense pixel-wise semantic segmentation. This is evident with occlusions due to projections onto 2D-pixel

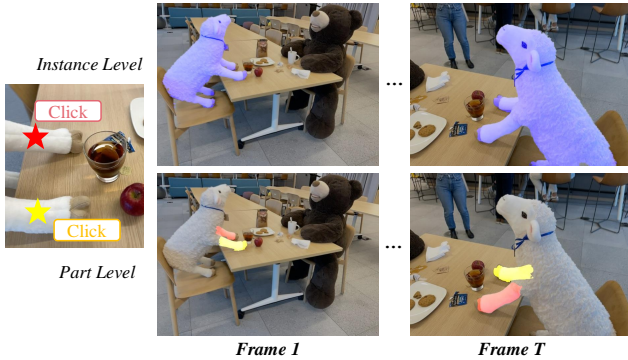


Figure 5. Cross-Level and Cross-Frame Segmentation Visualization. Our method accurately segments entire objects and individual finer parts with precise boundaries and 3D consistency.

w/ SuperG	w/ ins	w/ hier	mIoU $\uparrow$	mAcc. $\uparrow$
			10.12	14.49
✓			12.08	16.95
✓	✓		53.91	64.41
✓		✓	49.04	66.10
✓	✓	✓	<b>55.31</b>	<b>77.97</b>

Table 3. SuperG ablation study, *teatime* scene of LERF-OVS.

space. Without alpha blending, the occluded Gaussians cannot be effectively distinguished from one another. Instead, LangSplat [7] produces fine border segmentation but often includes incorrect semantic labels and noisy predictions, likely due to the lossy encoding of language information.

### 4.3. Results on the LERF-OVS Dataset

**Quantitative Results.** Although OpenGaussian attains a slightly higher mean Intersection over Union (mIoU), SuperGSeg surpasses it in mAcc, indicating more consistent and accurate pixel-wise classification. This suggests that SuperGSeg’s approach leads to more precise semantic labeling overall. SuperGSeg demonstrates robust performance across different scenes, excelling particularly in complex environments like *figurines* and *waldo kitchen*, where it achieves the highest mIoU among all methods. While OpenGaussian performs better in some scenes, SuperGSeg maintains competitive accuracy, reflecting its strong generalization capabilities. Overall, the superior mAcc of SuperGSeg highlights its ability to correctly classify a higher proportion of pixels. Unlike LangSplat and LEGaussians, which exhibit significantly lower performance, SuperGSeg offers substantial improvements, advancing open-vocabulary semantic segmentation tasks.

**Qualitative Results.** To illustrate the learned 3D language field, we first query the language features in 3D space and render them to 2D for visualization. As shown in Figure 3, our method achieves superior 3D localization without outliers and produces clearer boundaries. In scenes containing multiple objects, such as knives, OpenGaussian strug-

gles to localize all of them, whereas our method delivers finer segmentation results. Interestingly, the high-quality features learned by our SuperGSeg can distinguish the coffee mug from its content and the spoon inside of it. This demonstrates the effectiveness of our designs, such as the distillation of fine features into the Super-Gaussians.

**Multi-Granularity Segmentation.** We demonstrate our method’s capability to perform multi-granularity segmentation of the 3D scene using click-based visual prompts. Given a click on a reference image, SuperGSeg queries a small set of Super-Gaussians that have the same hierarchical features as the feature of the query pixel. These Super-Gaussians, which correspond to the part selected by the user, can then be rendered across different views. Furthermore, we use the instance feature of each SuperG to group into instances, allowing us to query the entire object with single click on one of its parts. We refer to this as a cross-level query. The cross-level query can also be performed top-down, where selecting an object with a single click automatically reveals its constituent parts.

**Ablation Study.** We conduct ablation studies on various components of our proposed method to validate the advantages of SuperG, as summarized in Table 3. For the baseline without SuperG, we train the language feature field using a similar approach described in Section 3.2. Additionally, we examine how different types of features affect SuperG learning. Specifically, we evaluate the performance of grouping SuperG based on anchor point coordinates and geometric features alone, as well as grouping using either the instance feature field or the hierarchical feature field individually. The experimental results reveal that learning language features per anchor point leads to suboptimal understanding in 3D space. In contrast, grouping similar anchors into SuperG significantly enhances performance. Crucially, both instance and hierarchical features are essential for accurate SuperG assignments. Relying solely on coordinates and geometric features results in overlapping SuperGs across objects with different semantics, leading to poor performance. In our complete configuration, which incorporates both instance and hierarchical features, we achieve optimal results.

## 5. Conclusion

This work introduced SuperGSeg, a novel approach for enhancing 3D scene understanding through a hierarchical, context-aware representation. Our framework leverages neural Gaussians to capture hierarchical segmentation features, which are then distilled into a sparse set of high-dimensional Super-Gaussians for advanced language-based feature rendering. With extensive experiments, we showed SuperGSeg’s superiority over prior works, thanks to its high-dimension language feature rendering and enhanced performance in open-ended 3D language query tasks.



# SuperGSeg: Open-Vocabulary 3D Segmentation with Structured Super-Gaussians

## Supplementary Material

In this supplementary document, we provide additional details about the proposed method. Specifically, We will first give more details on our Super-Gaussians approach in Section A, including the concept of superpoints, a detailed design of the Super-Gaussians module, and how this concept is used for downstream tasks. Then we discuss our evaluation protocol on the LERF-OVS dataset in Section B. We further explain additional implementation details on how to decode features from MLPs and OpenGaussians for 2D open-vocabulary semantic segmentation tasks in Section C. In addition, we report more ablation studies on the hyperparameters of Super-Gaussians in Section D. Finally, we discuss the limitations of our work and the future work for improvement in Section E.

### A. Concept of Super-Gaussians

**Preliminary: Superpoints.** The use of superpoints has been explored in various point cloud tasks, including semantic segmentation [30, 35–39], instance segmentation [39, 40], and object detection [39] and more recently in dynamic Gaussian Splatting [31]. Superpoints are effective in these tasks, and they have been used to improve the efficiency and accuracy of point cloud processing. On one hand, superpoints can be generated by aggregating points with similar geometric characteristics [41], and these superpoints can be used to construct a superpoint graph [35, 36, 42] which captures the spatial relationships between different instances. On the other hand, superpoints can be constructed using semantic information [30, 39]. By creating an association matrix, SPNet [30] forms superpoints that are distinctive in the semantic feature space. Following this approach, SP-GS [31] introduces superpoints to over-segment Gaussians within the temporal domain, enabling fine modeling of superpoints with dynamic properties.

In contrast to SP-GS, our method leverages the over-segmentation property of superpoints to either assign language features to the fine details of the scene or facilitate the assignment of high-dimensional language features, enabling full querying of text prompts.

**Module Design.** As Figure 7 depicts, our SuperG generating network consists of four learnable MLPs. More specifically, inspired by SPNet [30], we implement three mapping functions  $F_\phi$ ,  $F_\varphi$ ,  $F_\psi$  as MLPs. Each function is tailored to a specific difference in attributes, capturing complex and nuanced information about the relationship between an an-

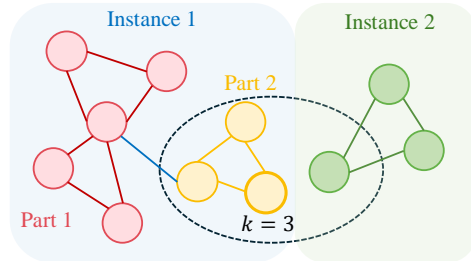


Figure 6. Examples of Super-Gaussian graph.

chor and its  $k$ -nearest Super-Gaussians independently and encoding the relevancy of that attribute (coordinate, segmentation, or geometry) for the Super-Gaussian assignment into a feature embedding. The final MLP  $F_{sg}$  takes the concatenation of three embeddings as input to integrate the spatial, semantic, and geometric differences into probabilistic assignments.

**Grouping Super-Gaussians for Instance and Hierarchical Segmentation.** As described in Section 3.3, after training the Super-Gaussian association modules outlined above, we generate the predicted soft association map, denoted as  $\hat{A} \in \mathbb{R}^{n \times k}$ . Each anchor point is assigned to one of its  $k$ -nearest neighbors based on the highest probability, resulting in the hard Super-Gaussian assignment, represented as  $\hat{A} \in \mathbb{R}$ . The attributes of these Super-Gaussians are then updated based on the hard assignments by computing the mean of the attributes of the anchor points assigned to each Super-Gaussian. These refined Super-Gaussians serve as the fundamental units for analyzing and interpreting the entire 3D scene.

Specifically, as depicted in Figure 6, we construct a graph where nodes represent Super-Gaussians. Given an instance similarity threshold  $\tau_{ins}$ , we determine that a Super-Gaussian and one of its  $k$ -nearest neighbors belong to the same instance if their instance feature similarity exceeds  $\tau_{ins}$ . These nodes are then connected by an edge.

Similarly, each instance is further divided into parts by constructing a Super-Gaussian graph within each instance and computing its connected components. The connectivity between nodes is defined based on the hierarchical feature similarity and a specified threshold  $\tau_{hier}$ . In our implementation, we set  $k = 3$  for nearest neighbor search,  $\tau_{ins} = 0.8$  for instance segmentation, and  $\tau_{hier} = 0.9$  for part segmentation.

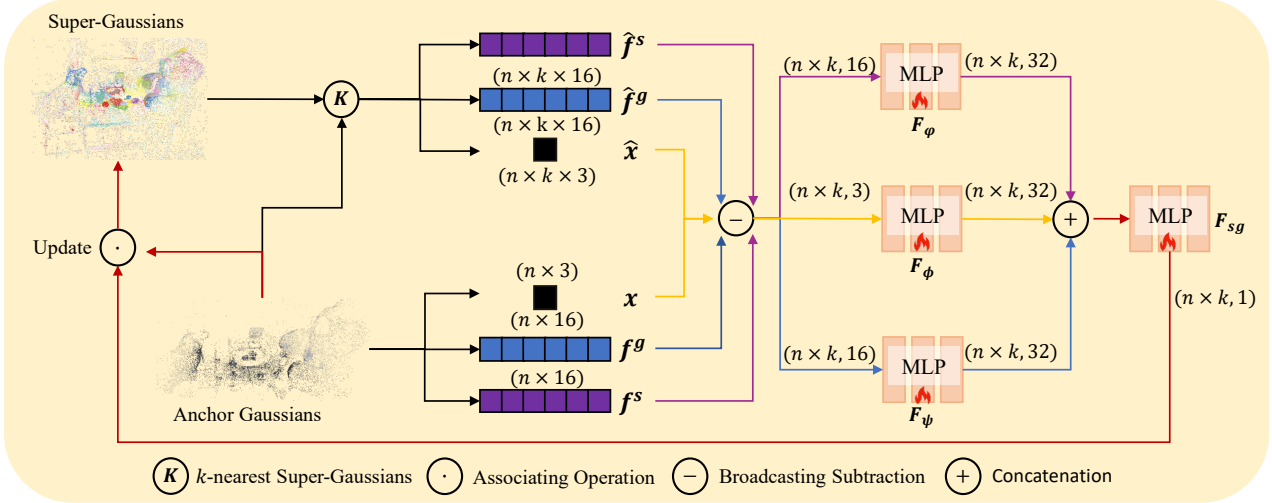


Figure 7. Detailed Illustration of Super-Gaussian Updating.

## B. Evaluation Details

**Evaluation Metrics on the LERF-OVS Dataset** We follow OpenGaussian [11] for the evaluation protocol on the LERF-OVS dataset. For each text query, we directly select the most relevant 3D Gaussians in 3D space and render the queried Gaussians into binary masks. The evaluation metrics include mIoU, which quantifies the overlap between the rendered mask and the ground truth object mask for the corresponding query, and accuracy, defined as the percentage of queries achieving an IoU greater than 0.25.

Notably, in our approach, we directly query the relevant Super-Gaussians instead of calculating relevancy scores and applying thresholds for each individual Gaussian [7]. This enables us to implement a unique voting strategy. Specifically, each selected Super-Gaussian votes for its respective instance. The relevancy score for each instance is then computed as the ratio of its selected Super-Gaussians to its total Super-Gaussian count. This allows us to query entire instances by text and render them to 2D binary masks. Leveraging the strong instance segmentation capabilities of Super-Gaussians, our open-vocabulary semantic segmentation results yield more complete masks and sharper boundaries, as shown in Figure 3.

## C. Additional Implementation Details

**Decoding Neural Gaussians from MLPs.** We use MLPs to decode the latent features. As shown in Figure 8, each MLP contains a hidden layer with a dimension of 32 located after the input layer. However, their decoding targets are different:  $F_I$  and  $F_H$  decode features for each anchor, while  $F_L$  decodes features for each Super-Gaussian. Specifically, the MLPs  $F_I$  and  $F_H$  take the anchor segmen-

tation feature  $f^s$  and anchor position  $x$  as inputs to predict instance feature  $g_i$  and hierarchical feature  $h_i$  of  $k$  neural Gaussians spawned per anchor point. In contrast, the MLP  $F_L$  predicts the CLIP-analogous feature  $l_s$  for each Super-Gaussian from the latent language feature  $f^l$  and the center  $\hat{x}$  of the Super-Gaussian.

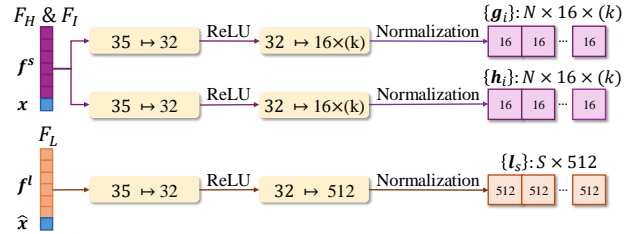


Figure 8. MLP structures to decode different features.

**OpenGaussian Implementation.** OpenGaussian [11] assigns language features to instance-level Gaussian Splatting, enabling direct language queries on 3D point clouds. However, this approach does not address 2D segmentation, making it less straightforward for 2D pixel-level semantic segmentation tasks on ScanNet. To still ensure a fair comparison, we first identify category-relevant 3D Gaussians by iterating over all text prompts to predict language feature maps for open-vocabulary semantic segmentation. For each instance-level Gaussian cluster, we determine the corresponding text prompt ID and store these IDs in a label map, which is then used to generate the final semantic segmentation. By following this approach, occlusions at the instance-level Gaussian are not explicitly handled, leading to the occlusion artifacts observed in Figure 4.

Ablation	mean		figurines		teatime		ramen		waldo_kitchen	
	mIoU	mAcc	mIoU	mAcc	mIoU	mAcc	mIoU	mAcc	mIoU	mAcc
$s = 250$	25.75	39.42	22.70	35.71	35.93	50.85	15.44	21.13	28.92	<b>50.00</b>
$s = 500$	34.05	50.03	27.44	48.21	<b>57.42</b>	<b>77.97</b>	<b>20.42</b>	<b>23.94</b>	<b>30.93</b>	<b>50.00</b>
$s = 1000$	<b>35.94</b>	<b>52.02</b>	<b>43.68</b>	<b>60.71</b>	55.31	<b>77.97</b>	18.07	<b>23.94</b>	26.71	45.45
$s = 2000$	27.61	40.60	27.64	46.43	47.58	62.71	12.46	16.90	22.76	36.36
$k = 3$	<b>35.94</b>	<b>52.02</b>	<b>43.68</b>	60.71	55.31	77.97	18.07	23.94	26.71	<b>45.45</b>
$k = 5$	33.70	46.76	21.59	35.71	<b>68.75</b>	<b>84.75</b>	16.96	21.13	27.48	<b>45.45</b>
$k = 10$	33.81	46.88	43.56	<b>62.50</b>	41.56	55.93	<b>21.82</b>	<b>28.17</b>	<b>28.31</b>	40.91

Table 4. Additional ablation studies on the LERF-OVS dataset [7] about the parameter choice for Super-Gaussian Attributes Updater. We use  $s = 1000$  Super-Gaussians and  $k = 3$  fr  $k$ -nearest neighbor in our implementation by default.

## D. Additional Ablation Studies

In Section 4, we perform ablation studies to evaluate the necessity of Super-Gaussians and analyze the performance of the instance feature field and hierarchical feature field. In this section, we further investigate the necessity of our proposed Super-Gaussian attributes updater and measure the impact of its individual components.

**Super-Gaussian Generation Approaches.** Given a pre-trained scene, our objective is to group anchor into meaningful Super-Gaussians using their coordinates, segmentation features, and geometric properties. We explore two alternative generation approaches. First, we evaluate a simple KMeans clustering algorithm by concatenating the aforementioned attributes and clustering them into  $k = 1000$  Super-Gaussians. Second, we experiment with a traditional supervoxel generation approach. In this method, we map the anchors to a point cloud, using the concatenated features as normals. We then apply the Voxel Cloud Connectivity Segmentation (VCCS) algorithm [43] to compute the Super-Gaussians. Finally, we compare these two non-learning-based approaches with our learning-based method for the Anchor-to-Super-Gaussian association.

We observed that KMeans fails to prevent the overlap of resulting Super-Gaussians across instances. Meanwhile, VCCS [43], originally designed for dense point clouds, struggles with the sparse structure of Gaussians. Its region-growing mechanism incorrectly clusters a large number of anchors together, which hinders the learning of the language feature field. The results in Table 5 show that our method is better suited for grouping Gaussians, achieving superior performance

**Super-Gaussian Attributes Updater.** As introduced in Section A, we employ three MLPs  $F_\phi$ ,  $F_\varphi$  and  $F_\psi$ , to capture the coordinate, segmentation, and geometric relationships between anchors and their  $K$ -nearest neighbors. To evaluate the contributions of these MLPs, we conduct an ablation study. Notably, in experiments where none of these

MLPs are used, we directly concatenate the differences of the attributes as input to  $F_{sg}$  for predicting the association matrix. The results presented in Table 6 demonstrate that each MLP contributes to improving the Super-Gaussian assignments. The MLP  $F_\varphi$ , which accounts for the segmentation feature differences between the anchor and the Super-Gaussian, has the most significant impact. Notably, using only  $F_\varphi$  yields a relatively high mIoU, emphasizing its effectiveness in aligning semantic features. However, our full setup that integrates the  $F_\phi$  and  $F_\psi$  for coordinate and geometric feature information further enhances mAcc. This suggests that incorporating additional spatial and geometric context refines the Super-Gaussian assignments, leading to more precise understanding of the scene.

**Parameters in Super-Gaussian Attributes Updater.** We conduct ablation studies on the parameters involved in generating Super-Gaussians using the Super-Gaussian Attributes Updater. One crucial parameter is the total number of Super-Gaussians predefined. Too few Super-Gaussians fail to distinguish all instances, causing a single Super-Gaussian to span multiple instances, which undermines semantic accuracy. Conversely, too many Super-Gaussians may introduce additional noise. Another parameter is the number of neighboring Super-Gaussians  $k$  considered for each anchor when computing the association matrix between anchors and Super-Gaussians.

As shown in Table 4, these two parameters are highly scene-specific, with the optimal number of Super-Gaussians  $s$  and neighbors  $k$  varying across different scenes. Notably, for fair comparisons, we use the same parameter values,  $s = 1000$  and  $k = 3$ , for all scenes. This parameter choice achieves optimal performance on average.

## E. Limitation

Despite the advancements achieved by our method, certain limitations remain. First, our approach inherits biases from the original visual foundation models, which constrains performance to a local maximum and may limit the generalization of results to diverse or unseen scenarios. Second,

Method	mIoU $\uparrow$	mAcc. $\uparrow$
Kmeans	53.77	67.80
VCCS[43]	0.45	0.00
Ours	<b>55.31</b>	<b>77.97</b>

Table 5. Super-Gaussian generation approaches ablation study on the *teatime* scene of LERF-OVS.

w/ $F_\phi$	w/ $F_\varphi$	w/ $F_\psi$	mIoU $\uparrow$	mAcc. $\uparrow$
			32.41	40.68
✓			48.29	67.80
	✓		<b>58.07</b>	75.66
		✓	37.12	62.71
✓	✓	✓	55.31	<b>77.97</b>

Table 6. Super-Gaussian Attributes Updater and components ablation study on the *teatime* scene of LERF-OVS.

our method is tailored for scene-specific language representation, requiring significant modeling time for each scene. This limits its applicability in tasks that demand rapid adaptation or broad generalization, such as in-the-wild scene understanding. Future work could focus on mitigating inherited biases and optimizing training pipelines to enhance scalability and generalization.

## References

- [1] Bernhard Kerbl, Georgios Kopanas, Thomas Leimkühler, and George Drettakis. 3d gaussian splatting for real-time radiance field rendering. *ACM Transactions on Graphics*, 42(4):139–1, 2023. 1, 2, 4
- [2] Ben Mildenhall, Pratul P Srinivasan, Matthew Tancik, Jonathan T Barron, Ravi Ramamoorthi, and Ren Ng. NeRF: Representing scenes as neural radiance fields for view synthesis. In *Proceedings of the European Conference on Computer Vision*, pages 405–421, 2020. 1, 2
- [3] Zehao Yu, Torsten Sattler, and Andreas Geiger. Gaussian opacity fields: Efficient and compact surface reconstruction in unbounded scenes. *arXiv preprint arXiv:2404.10772*, 2024. 1, 2
- [4] Pinxuan Dai, Jiamin Xu, Wenxiang Xie, Xinguo Liu, Huamin Wang, and Weiwei Xu. High-quality surface reconstruction using gaussian surfels. In *ACM SIGGRAPH 2024 Conference Papers*, pages 1–11, 2024.
- [5] Antoine Guédon and Vincent Lepetit. Sugar: Surface-aligned gaussian splatting for efficient 3d mesh reconstruction and high-quality mesh rendering. In *Proceedings of the IEEE/CVF Conference on Computer Vision and Pattern Recognition*, pages 5354–5363, 2024. 1, 2
- [6] Taoran Yi, Jiemin Fang, Zanwei Zhou, Junjie Wang, Guan-jun Wu, Lingxi Xie, Xiaopeng Zhang, Wenyu Liu, Xing-gang Wang, and Qi Tian. Gaussiandreamerpro: Text to manipulable 3d gaussians with highly enhanced quality. *arXiv preprint arXiv:2406.18462*, 2024. 1
- [7] Minghan Qin, Wanhua Li, Jiawei Zhou, Haoqian Wang, and Hanspeter Pfister. Langsplat: 3d language gaussian splatting. In *Proceedings of the IEEE/CVF Conference on Computer Vision and Pattern Recognition*, pages 20051–20060, 2024. 1, 2, 3, 4, 5, 6, 7, 8, 10, 11
- [8] Jin-Chuan Shi, Miao Wang, Hao-Bin Duan, and Shao-Hua Guan. Language embedded 3d gaussians for open-vocabulary scene understanding. In *Proceedings of the IEEE/CVF Conference on Computer Vision and Pattern Recognition*, pages 5333–5343, 2024. 4, 7
- [9] Shijie Zhou, Haoran Chang, Sicheng Jiang, Zhiwen Fan, Zehao Zhu, Dejia Xu, Pradyumna Chari, Suyu You, Zhangyang Wang, and Achuta Kadambi. Feature 3dgs: Supercharging 3d gaussian splatting to enable distilled feature fields. In *Proceedings of the IEEE/CVF Conference on Computer Vision and Pattern Recognition*, pages 21676–21685, 2024. 2, 3, 5, 7
- [10] Mingqiao Ye, Martin Danelljan, Fisher Yu, and Lei Ke. Gaussian grouping: Segment and edit anything in 3d scenes. In *Proceedings of the European Conference on Computer Vision*, pages 162–179, 2024. 3
- [11] Yanmin Wu, Jiarui Meng, Haijie Li, Chenming Wu, Yahoo Shi, Xinhua Cheng, Chen Zhao, Haocheng Feng, Errui Ding, Jingdong Wang, et al. Opengaussian: Towards point-level 3d gaussian-based open vocabulary understanding. *arXiv preprint arXiv:2406.02058*, 2024. 1, 2, 3, 6, 7, 10
- [12] Alec Radford, Jong Wook Kim, Chris Hallacy, Aditya Ramesh, Gabriel Goh, Sandhini Agarwal, Girish Sastry, Amanda Askell, Pamela Mishkin, Jack Clark, et al. Learning transferable visual models from natural language supervision. In *Proceedings of the International Conference on Machine Learning*, pages 8748–8763. PMLR, 2021. 1, 2, 3
- [13] Boyi Li, Kilian Q Weinberger, Serge Belongie, Vladlen Koltun, and Rene Ranftl. Language-driven semantic segmentation. In *International Conference on Learning Representations*, 2022. 1
- [14] Xingxing Zuo, Pouya Samangouei, Yunwen Zhou, Yan Di, and Mingyang Li. Fmgs: Foundation model embedded 3d gaussian splatting for holistic 3d scene understanding. *International Journal of Computer Vision*, pages 1–17, 2024. 2
- [15] Yanyan Li, Chenyu Lyu, Yan Di, Guangyao Zhai, Gim Hee Lee, and Federico Tombari. Geogaussian: Geometry-aware gaussian splatting for scene rendering. In *European Conference on Computer Vision*, pages 441–457. Springer, 2024. 2, 7
- [16] Alexander Kirillov, Eric Mintun, Nikhila Ravi, Hanzi Mao, Chloe Rolland, Laura Gustafson, Tete Xiao, Spencer Whitehead, Alexander C Berg, Wan-Yen Lo, et al. Segment anything. In *Proceedings of the IEEE/CVF International Conference on Computer Vision*, pages 4015–4026, 2023. 2, 3, 4
- [17] Yash Bhargat, Iro Laina, Joao F Henriques, Andrew Zisserman, and Andrea Vedaldi. Contrastive lift: 3d object instance segmentation by slow-fast contrastive fusion. *arXiv preprint arXiv:2306.04633*, 2023. 2
- [18] Zehao Yu, Anpei Chen, Binbin Huang, Torsten Sattler, and Andreas Geiger. Mip-splatting: Alias-free 3d gaussian splat-

- ting. In *Proceedings of the IEEE/CVF Conference on Computer Vision and Pattern Recognition*, pages 19447–19456, 2024. [2](#)
- [19] Binbin Huang, Zehao Yu, Anpei Chen, Andreas Geiger, and Shenghua Gao. 2d gaussian splatting for geometrically accurate radiance fields. In *ACM SIGGRAPH Conference*, pages 1–11, 2024. [2](#)
- [20] Tao Lu, Mulin Yu, Linning Xu, Yuanbo Xiangli, Limin Wang, Dahua Lin, and Bo Dai. Scaffold-gs: Structured 3d gaussians for view-adaptive rendering. In *Proceedings of the IEEE/CVF Conference on Computer Vision and Pattern Recognition*, pages 20654–20664, 2024. [2](#), [4](#), [7](#)
- [21] Justin Kerr, Chung Min Kim, Ken Goldberg, Angjoo Kanazawa, and Matthew Tancik. Lrf: Language embedded radiance fields. In *Proceedings of the IEEE/CVF International Conference on Computer Vision*, pages 19729–19739, 2023. [2](#), [3](#), [6](#)
- [22] Rahul Goel, Dhawal Sirikonda, Saurabh Saini, and PJ Narayanan. Interactive segmentation of radiance fields. In *Proceedings of the IEEE/CVF Conference on Computer Vision and Pattern Recognition*, pages 4201–4211, 2023. [2](#)
- [23] Sosuke Kobayashi, Eiichi Matsumoto, and Vincent Sitzmann. Decomposing nerf for editing via feature field distillation. *Proceedings of the International Conference on Neural Information Processing Systems*, 35:23311–23330, 2022.
- [24] Ayça Takmaz, Elisabetta Fedele, Robert W Sumner, Marc Pollefeys, Federico Tombari, and Francis Engelmann. Openmask3d: open-vocabulary 3d instance segmentation. In *Proceedings of the International Conference on Neural Information Processing Systems*, pages 68367–68390, 2023. [2](#)
- [25] Ashkan Mirzaei, Tristan Aumentado-Armstrong, Konstantinos G Derpanis, Jonathan Kelly, Marcus A Brubaker, Igor Gilitschenski, and Alex Levinstein. Spin-nerf: Multiview segmentation and perceptual inpainting with neural radiance fields. In *Proceedings of the IEEE/CVF Conference on Computer Vision and Pattern Recognition*, pages 20669–20679, 2023. [2](#)
- [26] Jiazhong Cen, Zanwei Zhou, Jiemin Fang, Wei Shen, Lingxi Xie, Dongsheng Jiang, Xiaopeng Zhang, Qi Tian, et al. Segment anything in 3d with nerfs. *Proceedings of the International Conference on Neural Information Processing Systems*, 36:25971–25990, 2023. [2](#)
- [27] Haiyang Ying, Yixuan Yin, Jinzhi Zhang, Fan Wang, Tao Yu, Ruqi Huang, and Lu Fang. Omniseg3d: Omniversal 3d segmentation via hierarchical contrastive learning. In *Proceedings of the IEEE/CVF Conference on Computer Vision and Pattern Recognition*, pages 20612–20622, 2024. [2](#), [4](#), [5](#)
- [28] Mathilde Caron, Hugo Touvron, Ishan Misra, Hervé Jégou, Julien Mairal, Piotr Bojanowski, and Armand Joulin. Emerging properties in self-supervised vision transformers. In *Proceedings of the IEEE/CVF International Conference on Computer Vision*, 2021. [3](#)
- [29] Matthias Zwicker, Hanspeter Pfister, Jeroen Van Baar, and Markus Gross. Ewa splatting. *IEEE Transactions on Visualization and Computer Graphics*, 8(3):223–238, 2002. [4](#)
- [30] Le Hui, Jia Yuan, Mingmei Cheng, Jin Xie, and Jian Yang. Superpoint network for point cloud oversegmentation. In *ICCV*, 2021. [5](#), [9](#)
- [31] Diwen Wan, Ruijie Lu, and Gang Zeng. Superpoint gaussian splatting for real-time high-fidelity dynamic scene reconstruction. In *Proceedings of the 41st International Conference on Machine Learning*, pages 49957–49972, 2024. [5](#), [9](#)
- [32] Angela Dai, Angel X. Chang, Manolis Savva, Maciej Halber, Thomas Funkhouser, and Matthias Nießner. Scannet: Richly-annotated 3d reconstructions of indoor scenes. In *Proceedings of the IEEE/CVF Conference on Computer Vision and Pattern Recognition*, 2017. [5](#), [6](#), [7](#)
- [33] Diederik Kingma and Jimmy Ba. Adam: A method for stochastic optimization. In *International Conference on Learning Representations (ICLR)*, 2015. [7](#)
- [34] Sara Fridovich-Keil, Alex Yu, Matthew Tancik, Qinhong Chen, Benjamin Recht, and Angjoo Kanazawa. Plenoxels: Radiance fields without neural networks. In *Proceedings of the IEEE/CVF conference on computer vision and pattern recognition*, pages 5501–5510, 2022. [7](#)
- [35] Loic Landrieu and Martin Simonovsky. Large-scale point cloud semantic segmentation with superpoint graphs. In *Proceedings of the IEEE conference on computer vision and pattern recognition*, pages 4558–4567, 2018. [9](#)
- [36] Damien Robert, Hugo Raguét, and Loic Landrieu. Efficient 3d semantic segmentation with superpoint transformer. In *Proceedings of the IEEE/CVF International Conference on Computer Vision*, pages 17195–17204, 2023. [9](#)
- [37] Damien Robert, Hugo Raguét, and Loic Landrieu. Scalable 3d panoptic segmentation as superpoint graph clustering. In *2024 International Conference on 3D Vision (3DV)*, pages 179–189. IEEE, 2024.
- [38] Loic Landrieu and Guillaume Obozinski. Cut pursuit: Fast algorithms to learn piecewise constant functions on general weighted graphs. *SIAM Journal on Imaging Sciences*, 10(4):1724–1766, 2017.
- [39] Yun Zhu, Le Hui, Yaqi Shen, and Jin Xie. Spgroup3d: Superpoint grouping network for indoor 3d object detection. In *Proceedings of the AAAI Conference on Artificial Intelligence*, volume 38, pages 7811–7819, 2024. [9](#)
- [40] Mingmei Cheng, Le Hui, Jin Xie, and Jian Yang. Sspc-net: Semi-supervised semantic 3d point cloud segmentation network. In *Proceedings of the AAAI conference on artificial intelligence*, volume 35, pages 1140–1147, 2021. [9](#)
- [41] Linghua Tang, Le Hui, and Jin Xie. Learning inter-superpoint affinity for weakly supervised 3d instance segmentation. In *Proceedings of the Asian Conference on Computer Vision*, pages 1282–1297, 2022. [9](#)
- [42] Loic Landrieu and Mohamed Boussaha. Point cloud oversegmentation with graph-structured deep metric learning. In *Proceedings of the IEEE/CVF Conference on Computer Vision and Pattern Recognition*, pages 7440–7449, 2019. [9](#)
- [43] Jeremie Papon, Alexey Abramov, Markus Schoeler, and Florentin Worgotter. Voxel cloud connectivity segmentation-supervoxels for point clouds. In *Proceedings of the IEEE conference on computer vision and pattern recognition*, pages 2027–2034, 2013. [11](#), [12](#)